ELSEVIER

Global and Planetary Change 32 (2002) 331–347

GLOBAL AND PLANETARY CHANGE

www.elsevier.com/locate/gloplacha

A comparison of simulated monsoon circulations and snow accumulation in Asia during the mid-Holocene and at the Last Glacial Maximum

Andrew B.G. Bush

Department of Earth and Atmospheric Sciences, University of Alberta, 126 Earth Science Building T6G 2E3 Edmonton, Alberta, Canada

Accepted 16 October 2001

Abstract

Tropical climatology through the last glacial cycle is believed to have ranged from colder, windier conditions at the Last Glacial Maximum (LGM) to relatively warm, stable conditions during the Holocene. Changes in strength of the South Asian monsoon have previously been determined from a variety of proxy data and have been attributed primarily to changes in radiative forcing, although tropical sea surface temperature (SST) is known to play a fundamental role in regulating monsoon strength and is also believed to have changed throughout the late Quaternary.In this study, the monsoons simulated in a coupled atmosphere–ocean general circulation model (GCM) configured for the mid-Holocene (6000 years B.P.) and for the LGM (21,000 years B.P.) are compared. The colder and windier conditions simulated for the LGM produced a summer monsoon whose westerly winds are stronger and whose precipitation and snowfall into the eastern Himalaya are increased, with drier conditions over the rest of the Indian subcontinent and over most of southwest Asia.The mid-Holocene monsoon circulation is stronger than today, and annual mean snow accumulation is increased over the northwestern Himalaya. These changes in precipitation and snow accumulation are analyzed in terms of the altered atmospheric circulations, which are in turn driven by changes in radiative forcing, sea surface temperatures, and sea surface height. All of these factors are therefore demonstrated to be important in governing the spatial distribution of snow and ice deposition in the Himalaya during the late Quaternary, and are likely to have contributed to the observed asynchroneity of Himalayan glaciation and Northern Hemisphere ice sheet volume.

Keywords: Last Glacial Maximum and Holocene monsoons; numerical simulations; glaciation in Asia

1. Introduction

Accumulation of snow and ice in the Himalaya is highly dependent on the dynamics of both the summer and winter South Asian monsoon, as well as on the strength and position of the midlatitude westerly jet and the annual mean circulation patterns. It is the intricate interplay between monsoon winds, the westerly jet, available moisture, surface albedo, and orography that governs regional deposition in the modern monsoon (Hahn and Shukla, 1976; Dey and Bhanu Kumar, 1982; Dickson, 1984; Dey et al., 1985; Meehl, 1997). To complicate matters further, however, winds and moisture fluxes are strongly dependent on tropical sea surface temperatures (SSTs) in the Pacific and

E-mail address: andrew.bush@ualberta.ca (A.B.G. Bush).

0921-8181/02/$ - see front matter
PII: S0921-8181(02)00074-7

Indian Oceans and hence show distinct interannual fluctuations that correlate with the El Niño Southern Oscillation (e.g., Keshavamurty, 1982; Rasmusson and Carpenter, 1983; Soman and Slingo, 1997; Torrence and Webster, 1999; Shrestha et al., 2000).

It is also known, through both proxy data and direct numerical simulations, that all of these climatic variables have changed in the Earth's past, particularly in the late Quaternary since the Last Glacial Maximum (e.g., Kutzbach and Otto-Bliesner, 1982; Prell and Kutzbach, 1992; Wright et al., 1993; Benn and Owen, 1998; Bush and Philander, 1999). During the early–mid-Holocene, for example, a change of Earth's angle of obliquity combined with a boreal summertime perihelion to produce a stronger seasonal cycle in the Northern Hemisphere. This altered radiative forcing drove stronger monsoon winds and increased upwelling in the Arabian Sea (e.g., Kutzbach and Otto-Bliesner, 1982; Prell, 1984; Kutzbach and Guetter, 1986; Prell and Kutzbach, 1992). During the Last Glacial Maximum, on the other hand, the global circulation appears to have been stronger (Sarnthein et al., 1981; Pedersen, 1983) and from sediment deposits in the Arabian Sea it appears that the monsoon circulation was different (e.g., Sirocko et al., 1991). In addition, proxy data and numerical simulations with coupled atmosphere–ocean GCMs suggest changes in mean tropical SST during the late Quaternary that are likely to have been large enough to have played a role in regulating monsoon winds and precipitation (e.g., Lyle et al., 1992; Guilderson et al., 1994; Bush and Philander, 1998; Bush, 1999; Otto-Bleisner, 1999).

Further, there appears to be spatial as well as temporal variability to glacier expansion within the Himalaya. During the mid-Holocene, for example, glaciers expanded in the northwestern Himalaya, but at the LGM growth was limited (Phillips et al., 2000; Taylor and Mitchell, 2000). Conversely, glaciers underwent significant expansion in the eastern Himalaya at the LGM (Richards et al., 2000). It has therefore been suggested that the observed asynchroneity between glacier advance in some regions of the Himalaya and Northern Hemisphere ice sheet volume may be related to changes in monsoon circulation and moisture transport (Benn and Owen, 1998; Richards et al., 2000; Phillips et al., 2000). It is therefore important to understand, first, how monsoon circulations changed in the late Quaternary, and second, the dynamical reasons for these changes. In order to address this question, we compare and contrast monsoon circulations, freshwater fluxes, and snow accumulation during the mid-Holocene and at the LGM as they are predicted by a coupled atmosphere–ocean GCM.

The outline of the paper is as follows. Section 2 gives a brief description of the numerical model that is used to perform the simulations. Section 3 describes the results for the summer monsoon, and Section 4 describes the results for the winter monsoon. A discussion and comparison to observations follow in Section 5, and conclusions are presented in Section 6.

2. The model

The main features of the model will be outlined only briefly here because full details of the simulations have been described elsewhere (Bush and Philander, 1999 for the LGM; Bush, 1999 for the mid-Holocene). Both simulations were performed with a coupled atmosphere–ocean GCM whose atmospheric component is detailed in Gordon and Stern (1982), and whose oceanic component is detailed in Pacanowski et al. (1991). The model is global with an equivalent atmospheric resolution of 3.75° in longitude, 2.25° in latitude (at the equator), and 14 levels in the vertical. The ocean model has a comparable resolution of 3.62° in longitude and 2° in latitude with 15 levels in the vertical, most of which are in the upper ocean. Sea ice is computed according to the thermodynamic formulation of Fanning and Weaver (1996) with a sea ice albedo parameterization that is dependent on ice thickness. The models are coupled with dynamical and thermodynamical communication at 1-day intervals. The atmospheric model receives daily mean SST, surface current velocities, and sea ice extent; the ocean model receives daily mean vector wind stress, net heat flux, net freshwater flux, net shortwave radiation, and sea ice extent.

In the mid-Holocene simulation, modern values of atmospheric CO_2, topography, sea level, and bare land surface albedo are imposed. Seasonal solar insolation is computed using the orbital parameters of obliquity, eccentricity, and longitude of perihelion appropriate for 6000 B.P. (Berger and Loutre, 1991; Berger, 1992).

In the LGM simulation, atmospheric CO_2 levels are reduced to 200 ppm, seasonal insolation is com-

puted as appropriate for 21,000 B.P., LGM ice sheet topography is imposed (Peltier, 1994), and continental margins are set assuming a 120-m drop in sea level (Fairbanks, 1989). Bare land surface albedo is also set for the LGM (CLIMAP, 1981) but may be modified by snowfall during the integration.

For reference, July and December insolation curves for 30°N are shown in Fig. 1, with the times of the simulations indicated. At this latitude, insolation at the LGM is approximately the same as today. Increased seasonality (i.e., more insolation in July and less in December) is evident through much of the past 150,000 years, particularly during the Holocene and ~128,000 years B.P.

In both simulations, the ocean is initially at rest with temperature and salinity fields specified from modern observational data (Levitus, 1982). The LGM simulation is 15 years long with results averaged over the last 5 years; the mid-Holocene simulation is 26 years long with results averaged over the last 16 years. The 10-year spin-up time is sufficient to allow the surface oceans to equilibrate to the altered atmos-

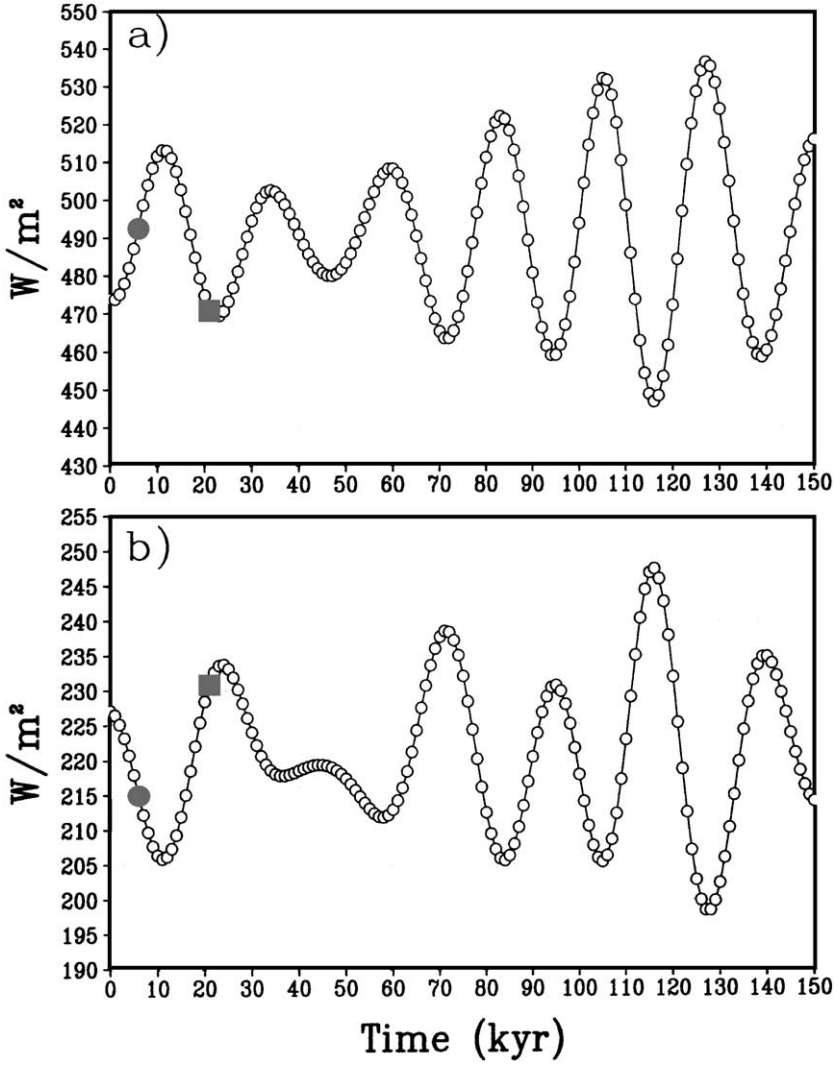

Fig. 1. Insolation at 30°N over the past 150,000 years for (a) July and (b) December. The times of the simulations are marked with grey circles (mid-Holocene) and grey squares (LGM). Data are from Berger and Loutre (1991).

pheric winds and radiative forcing, and for the tropical thermocline to alter its mean state (see Bush and Philander, 1998; 1999). Results are compared to a 40-year control simulation that is configured for the present day.

3. Results for the summer monsoon

During the boreal summer months of June–July–August (JJA), monsoon winds on the 900 mb surface exhibit a stronger southwesterly Somali jet over the Arabian Sea in both the mid-Holocene and LGM simulations (Fig. 2). During the mid-Holocene, there is enhanced anticyclonic flow over the Indian Ocean that is in the same direction as the modern monsoon winds (compare Fig. 2a,b). At the LGM, differences in simulated wind speeds are much greater and there is nearly a doubling of wind speed over the Bay of Bengal (Fig. 2c). Along the equator, wind differences indicate a weakening of the equatorial easterlies at the LGM. The LGM westerly wind anomalies are driven in part by low-level convergence over the Indonesian region. This convergence arises because lower LGM sea level exposes the extensive Sunda shelf (the continental shelf that joins the islands of the Indonesian archipelago), which acts as a site for strong tropical convection.

A reduction in freshwater flux (precipitation minus evaporation) occurs over much of the equatorial Indian Ocean in both simulations, primarily as a result of decreased precipitation (Fig. 3). Evaporation over the Indian Ocean also decreases in both simulations, but only to a maximum value of ~10% of modern during the mid-Holocene, so it does not compensate for the precipitation changes. Decreased evaporation in the mid-Holocene simulation is caused by cooler SST along the equator (approximately 0.5° cooler; see Fig. 10 below) which in turn is caused by stronger wind-driven upwelling (and not by changes in short wave radiation). In the LGM simulation, decreased evaporation is caused by a combination of reduced easterly wind speeds as well as by longwave radiative cooling of the upper ocean because of reduced atmospheric CO_2 and water vapor content (JJA Indian Ocean SSTs are approximately 2.5° colder in the LGM simulation). Freshwater flux into the northern Indian Ocean, on the other hand, is greater than today during the mid-Holocene but smaller at the LGM (with the exception of the Bay of Bengal, where it is greater).

Freshwater flux over the continental landmasses is quite different, however. In the mid-Holocene simulation, freshwater flux increases across much of South Asia and East Africa whereas it is reduced in these regions at the LGM (compare Fig. 3b,c). However, both simulations exhibit large summertime precipitation anomalies in the eastern Himalaya, with a second maximum over Thailand at the LGM. The strong westerly winds simulated at the LGM therefore dry the central and western region of India and increase precipitation over the eastern Himalaya, China, and northern Indonesia.

The colder climate at the LGM increases dramatically the summertime snowfall over the eastern Himalaya (Fig. 4). Snowfall during the mid-Holocene, however, is slightly reduced across the entire front range of the Himalaya because JJA temperatures are approximately 1.5–2° warmer than today (Fig. 4b). In terms of summertime snow accumulation and glacier expansion, therefore, changes in the JJA monsoon appear to be more important at the LGM than during the mid-Holocene. However, changes in mid-Holocene annual mean snow accumulation will be shown in the discussion to be greater than today, particularly in the northwestern Himalaya.

4. Results for the winter monsoon

December–January–February (DJF) northeasterly monsoon winds across the northern Indian Ocean are stronger in both the mid-Holocene and LGM simulations (Fig. 5). As was the case for the summer monsoon, wind differences in the LGM simulation are greater and exhibit convergence over the Sunda shelf with westerly wind anomalies over the equatorial Indian Ocean that weaken the equatorial easterlies. In the mid-Holocene simulation the trade easterlies are also slightly weakened south of the equator. Colder temperatures over the Indian subcontinent at the LGM induce a relatively strong anticyclonic flow over India that increases convergence along the central-western Himalaya. These winds transport moisture from the Bay of Bengal and the eastern Arabian Sea northwards to the front range and thereby increase wintertime precipitation (Fig. 6).

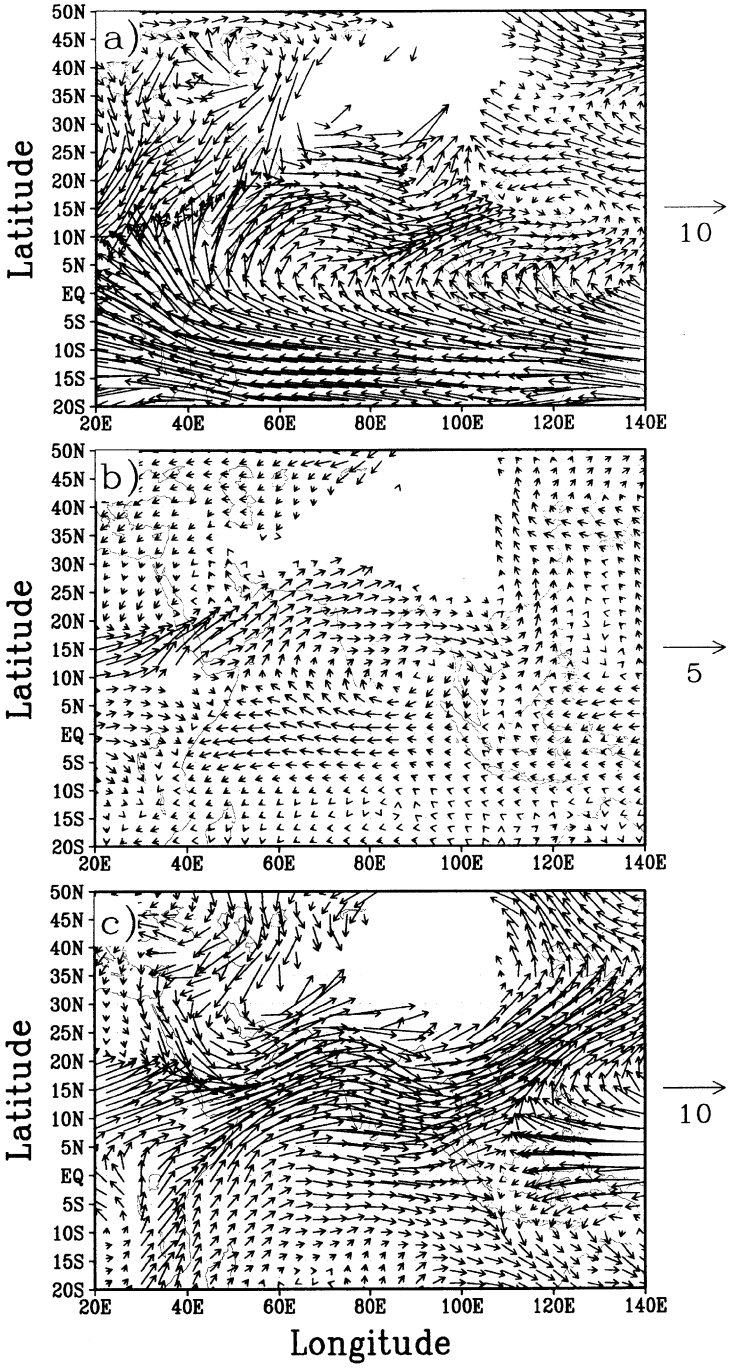

Fig. 2. (a) June–July–August (JJA) winds on the 900 mb surface in the control simulation. Differences in these winds (experiment minus control) are shown for (b) the mid-Holocene, and (c) the Last Glacial Maximum (LGM). No vectors are shown when the pressure surface is intersected by the Earth's surface. Units are m/s as indicated. Note that the wind vectors in (b) are scaled differently.

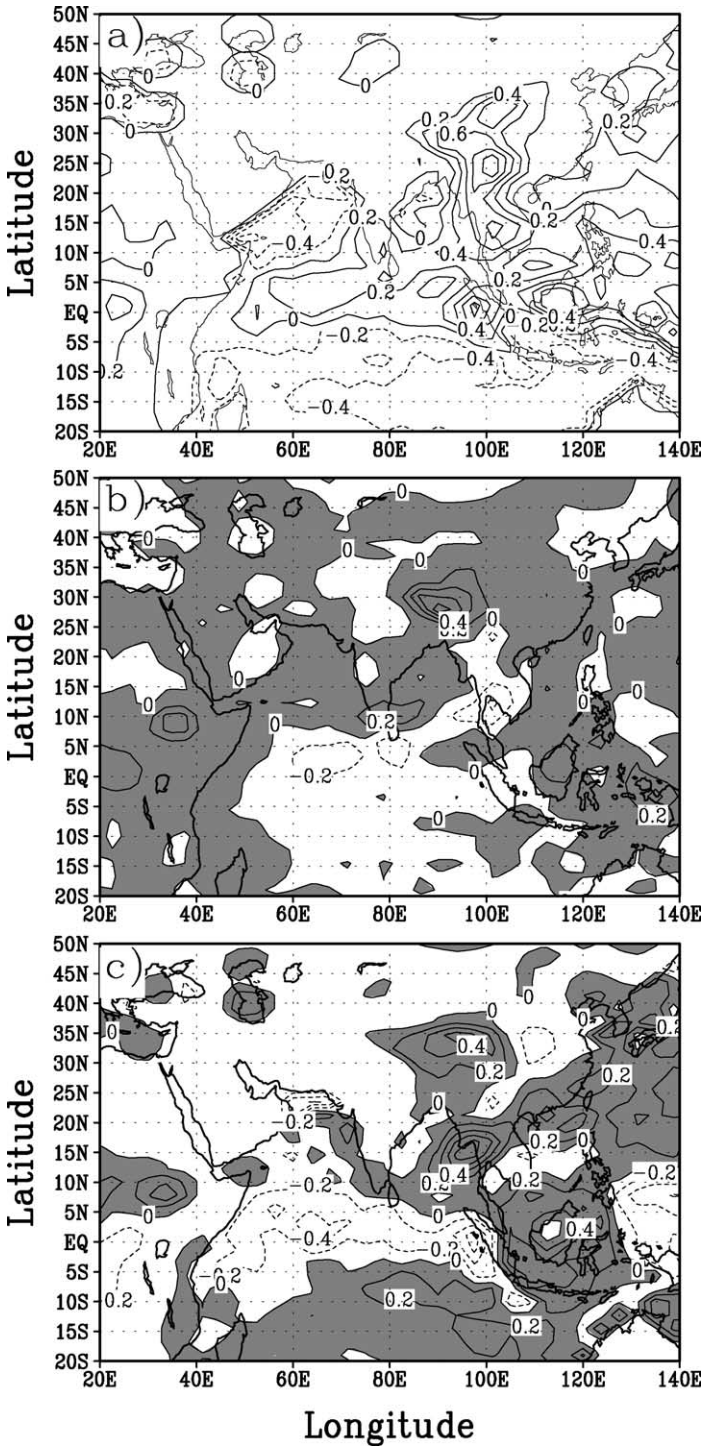

Fig. 3. (a) JJA net freshwater flux (precipitation minus evaporation) in the control simulation. Differences (experiment minus control) are shown for (b) the mid-Holocene, and (c) the Last Glacial Maximum (LGM) with grey shading indicating regions that are wetter than today. Units are cm/day, with a contour interval of 0.2 cm/day in all panels.

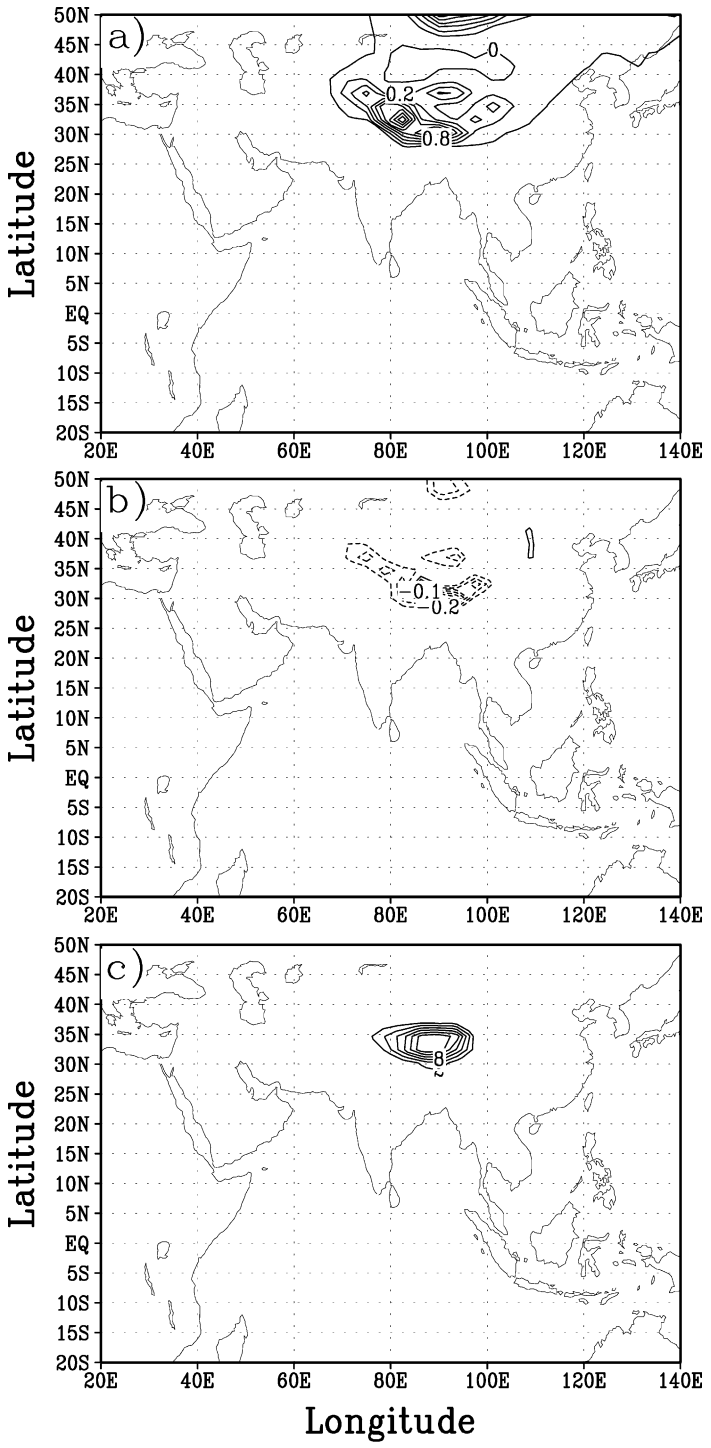

Fig. 4. (a) JJA snow accumulation in the control simulation, and differences (experiment minus control) in (b) the mid-Holocene simulation and (c) the LGM simulation. Units are cm water equivalent. The contour interval is 0.2 cm in (a), 0.1 cm in (b), and 3 cm in (c).

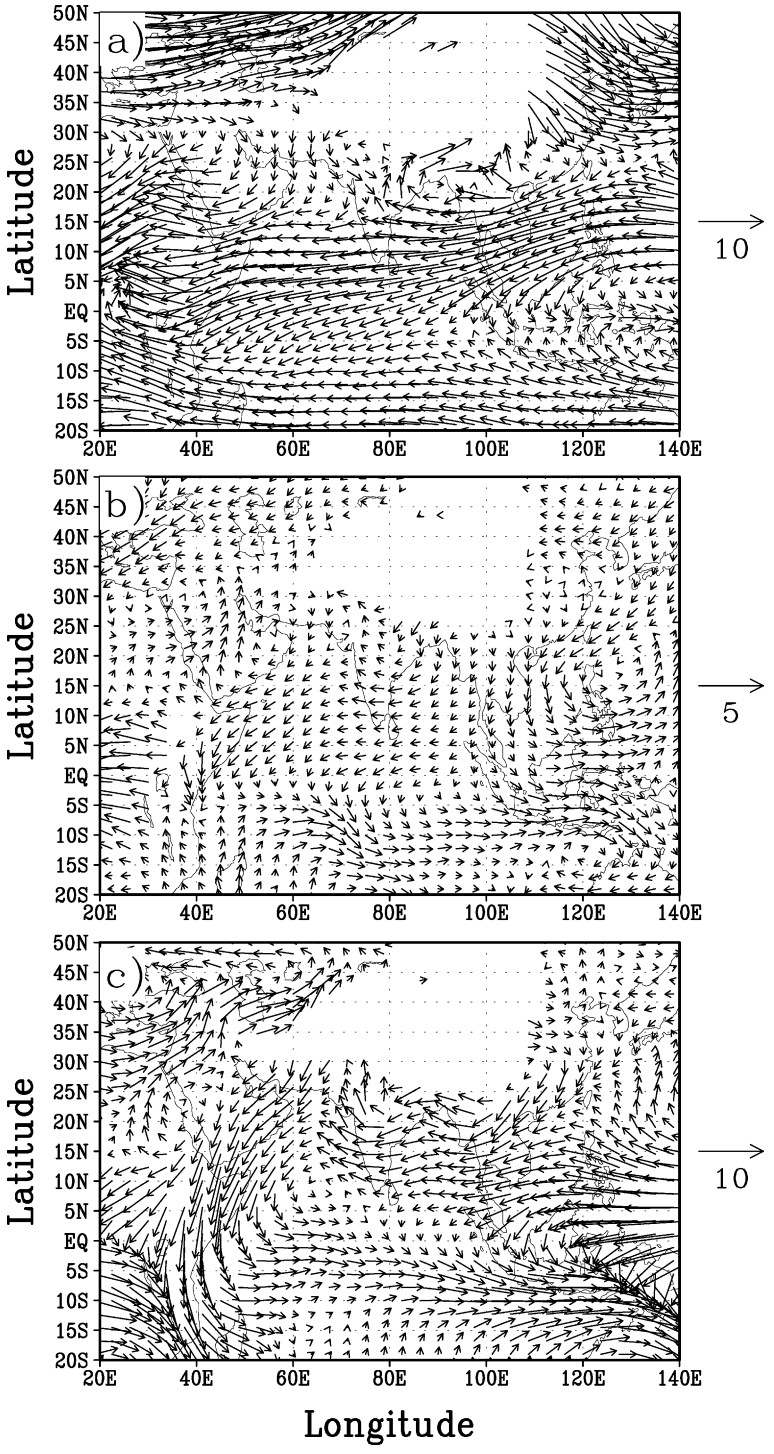

Fig. 5. December–January–February (DJF) mean winds on the 900 mb surface. The layout is as in Fig. 2. Units are m/s and scaled as shown. Note that the wind vectors in (b) are scaled differently.

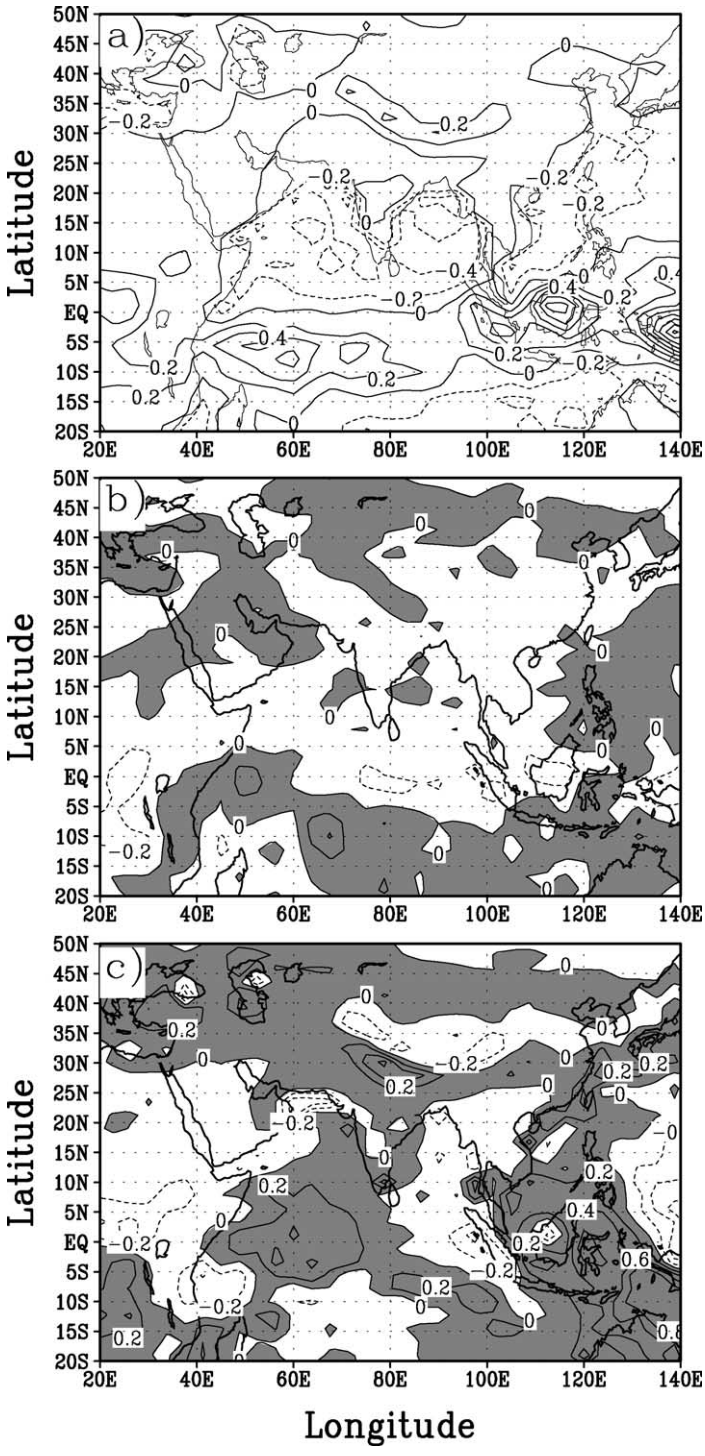

Fig. 6. (a) DJF net freshwater flux (precipitation minus evaporation) in the control simulation. Differences (experiment minus control) are shown for (b) the mid-Holocene, and (c) the Last Glacial Maximum (LGM) with grey shading indicating regions that are wetter than today. Units are cm/day, with a contour interval of 0.2 cm/day in all panels.

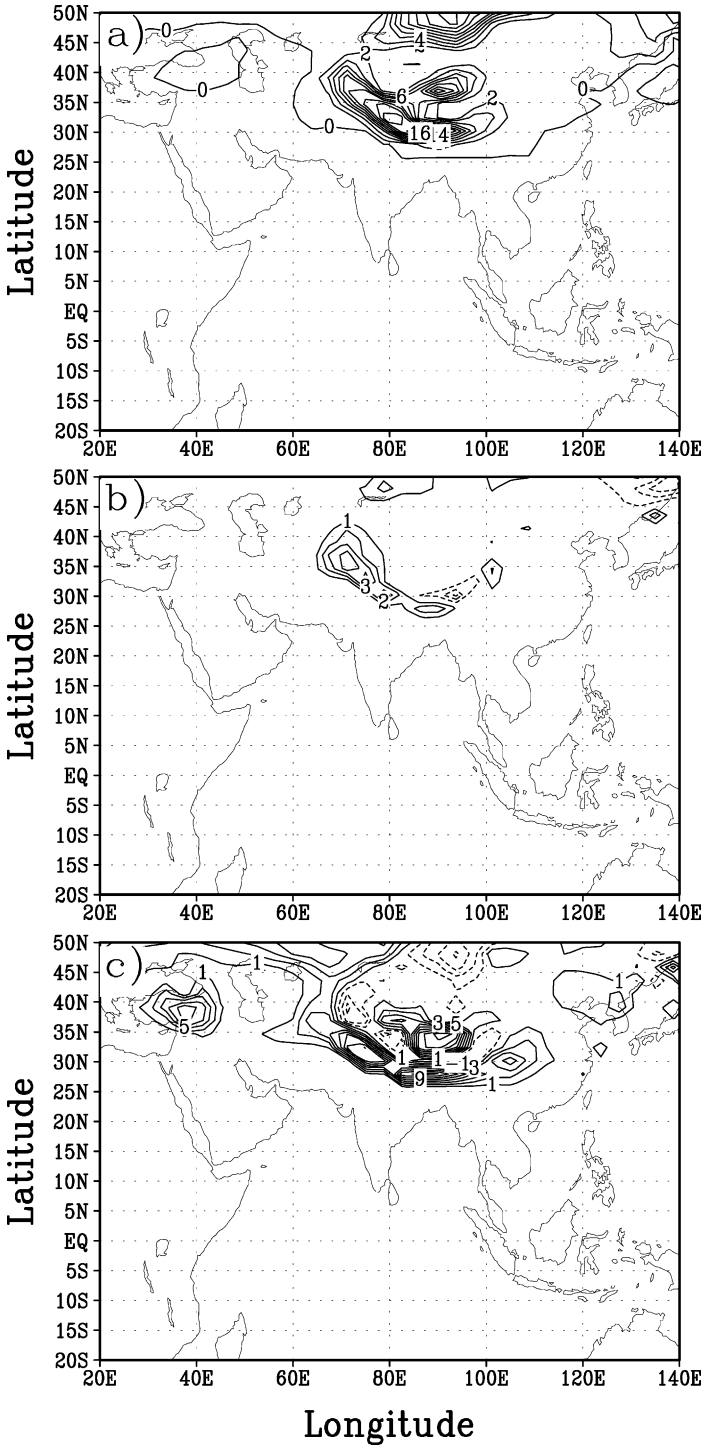

Fig. 7. (a) DJF snow accumulation in the control simulation, and differences (experiment minus control) (b) in the mid-Holocene and (c) at the LGM. Units are cm water equivalent. The contour interval is 2 cm in (a) and (c), and 1 cm in (b).

There is also a large increase in DJF freshwater flux over the exposed Sunda shelf and over the equatorial Indian Ocean because of increased convection in this area. In the mid-Holocene simulation, on the other hand, there is very little additional freshwater flux over the Himalaya because most of the anomalous wintertime precipitation falls as snow.

DJF temperatures over the Himalaya are colder than today in both simulations, and as a result there is larger wintertime snow accumulation (Fig. 7). During the mid-Holocene, snowfall differences are greatest in the northwestern Himalaya although there is more accumulation than today across the entire front range (Fig. 7b). Analysis of the 750 mb winds indicate enhanced convergence over this region of a westerly wind anomaly flowing over the Arabian Peninsula and the Gulf of Oman. These winds are part of an anticyclonic circulation anomaly that is centered over the southern tip of the Arabian Peninsula, which is $\sim 1.5-2^\circ$ colder during the mid-Holocene. (Although it is weaker at the 950 mb level, this anticyclonic circulation can be seen in Fig. 5b.)

In the LGM simulation, DJF snowfall differences stretch across the entire front range and suggest a broad expansion of LGM wintertime snow cover, particularly all along the front range and over the Tibetan Plateau (with regions of decreased accumulation in between). The surface area of positive snow accumulation is much greater in the LGM simulation (compare Fig. 7a,c), with new regions of positive accumulation in the northwestern Himalaya, over the region of the Taklimakan Desert, as well as over the eastern Himalaya and northwestern China. Since topography in the model is spectrally smoothed at the resolution employed, simulated spatial variations of snow accumulation will only reflect the large-scale changes in atmospheric circulation. Field measurements should, of course, exhibit a much higher degree of spatial variability with much more local topographic effects. However, the model results should give an overall picture of how the large-scale accumulation rates were different.

5. Discussion

Analysis of the seasonal monsoons indicates that wind, freshwater, and snowfall changes in the LGM simulation are greater than those in the mid-Holocene simulation. However, for comparison to proxy data such as reconstructions of glacier extent it is the annual mean quantities that are most relevant (although seasonal averages are necessary to diagnose contributions to the annual mean).

Wind anomalies during the mid-Holocene are stronger in the summertime than in the wintertime and hence dominate the annual mean difference (Fig. 8). There is therefore a simulated $\sim 83\%$ increase in upwelling off the Arabian Peninsula near 18°N. This result agrees with inferences made from biogenic opal that there was much more productivity in this area at this time (e.g., Prell, 1984; Prell and van Campo, 1986; Prell and Kutzbach, 1992). On the other hand, wind anomalies over the Arabian Sea at the LGM are in the opposite direction in summer and winter but are of comparable strength (cf. Figs. 2c and 5c). In an annual mean there is therefore not a large change in alongshore wind speed over this region (Fig. 8c), although between 16°N and 21°N a reduction in alongshore winds does decrease upwelling by 18%. However, over the Gulf of Oman and further east, alongshore winds are comparable to if not stronger than today, with concomitant changes in annual mean upwelling. There is evidence for the persistence of high accumulation rates of organic carbon in this region during glacial times (Sarnthein and Winn, 1990).

Simulated JJA northwesterly winds over the Arabian Peninsula are stronger at the LGM than today (cf. Fig. 2c). This result supports the suggestion that it was enhanced northwesterlies from central Arabia that brought more (and larger) lithogenic sediments to the northwestern Arabian Sea and which produced the characteristic northwest–southeast deposition pattern that is observed for the LGM (Sirocko et al., 1991; Clemens and Prell, 1990).

Annual mean freshwater flux over the Himalaya was not substantially different from today (not shown) even though there are seasonal differences (cf. Figs. 3 and 6). This lack of change in net freshwater flux may contribute to the stability of large river outflow in this region that has been inferred for the Quaternary (Metivier and Gaudemar, 1999). However, simulated changes in snow accumulation are also likely to increase river discharge to the Arabian Sea (Prins and Postma, 2000) and to the Bay of Bengal (Cullen, 1981) but may not have lasted a sufficiently long time

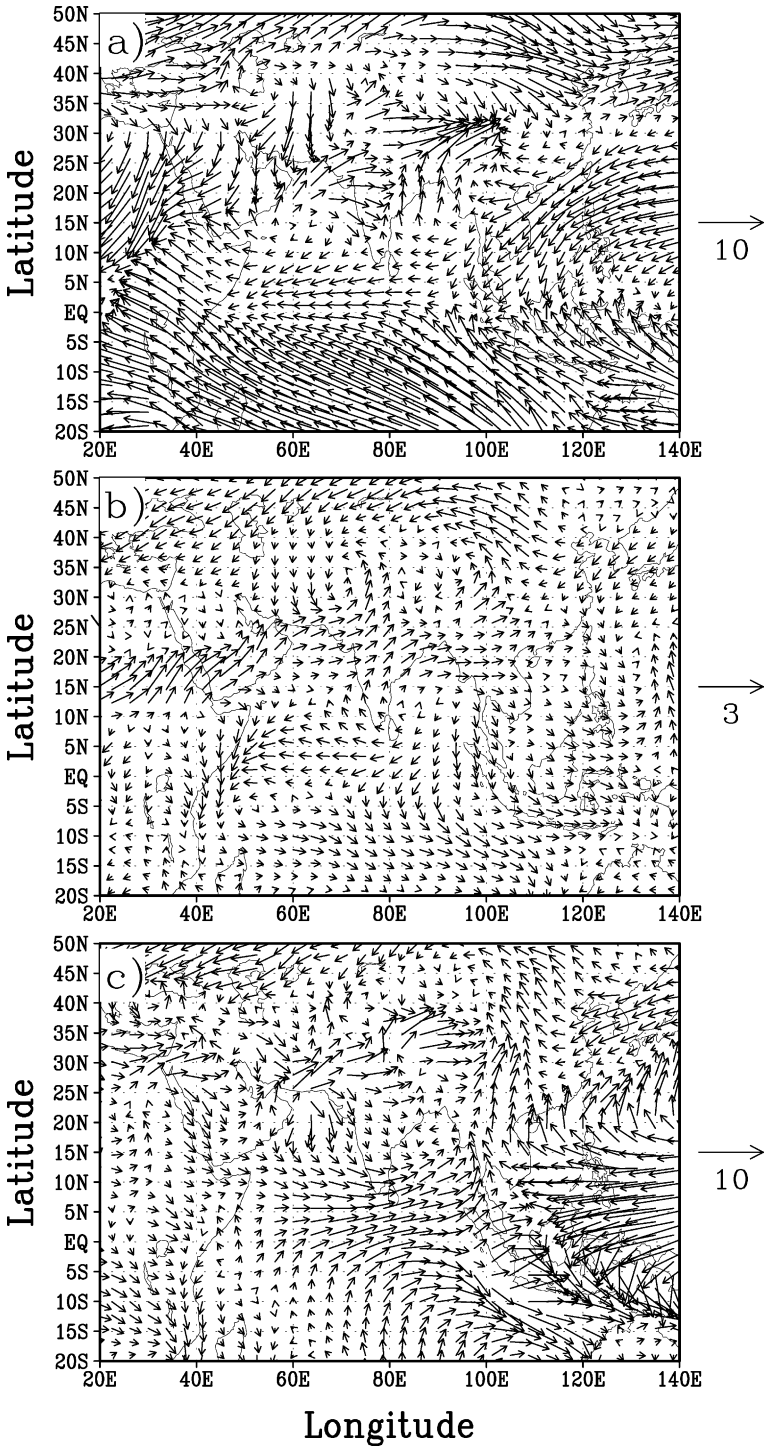

Fig. 8. Annual mean winds on the 900 mb surface. The layout is as in Fig. 2. Units are m/s and scaled as shown. Note that the wind vectors in (b) are scaled differently.

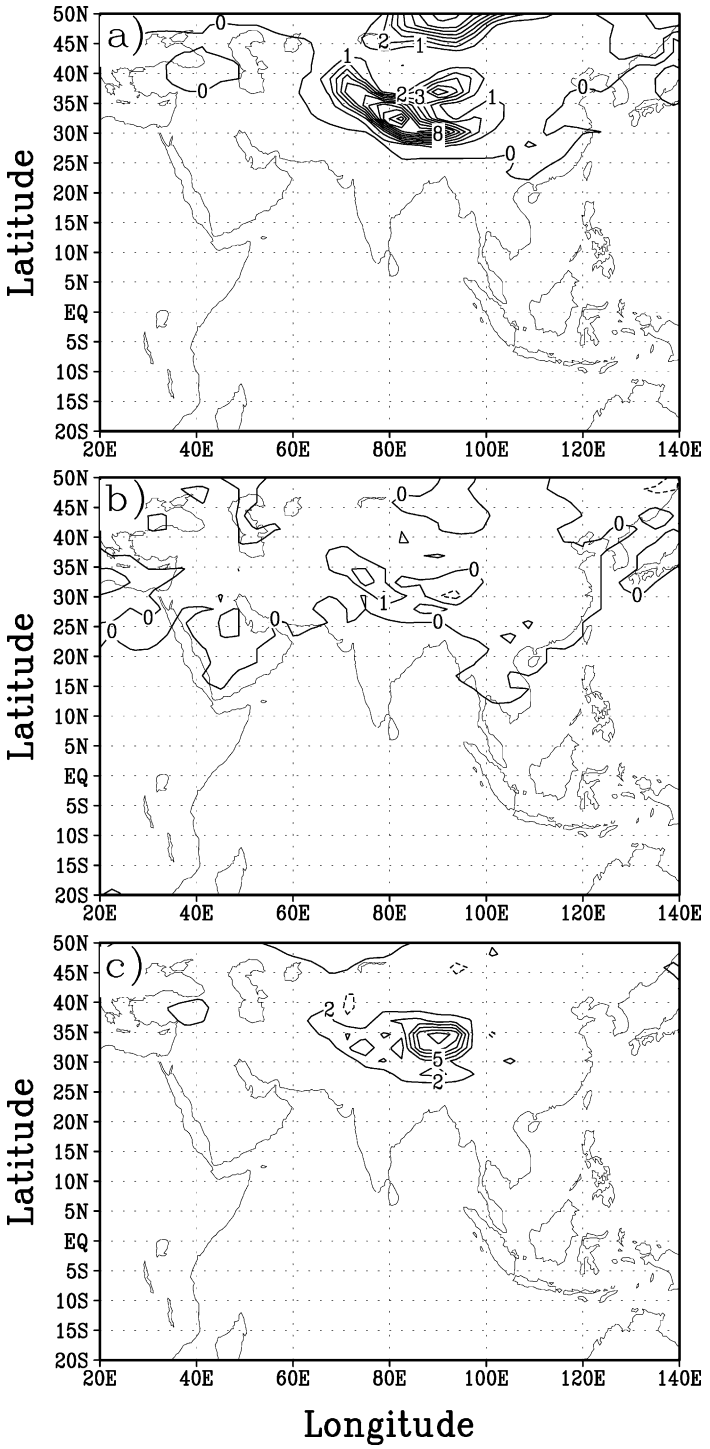

Fig. 9. Annual mean snow accumulation. The layout is as in Fig. 4. Units are cm water equivalent with a contour interval of 1 cm in all panels.

to have significantly perturbed the alluvial plains (Metivier and Gaudemar, 1999).

At the LGM, one difference in the winds that persists both through summer and winter is the reduction in strength of the easterlies over the equatorial Indian Ocean. The exposed Sunda shelf and the tropical convection that it produces — particularly in the equinox months of March and September — creates strong low-level convergence in the annual mean (Fig. 8c). These convergent winds create a southerly jet over northern Indonesia that converges onto the eastern Himalaya, contributing to the large annual mean snow accumulation there (Fig. 9). Therefore, enhanced westerlies of the JJA summer monsoon (which are evident in the annual mean wind anomalies) combine with this increased southerly flow from the Sunda shelf to produce the large annual mean snow accumulation in the eastern Himalaya.

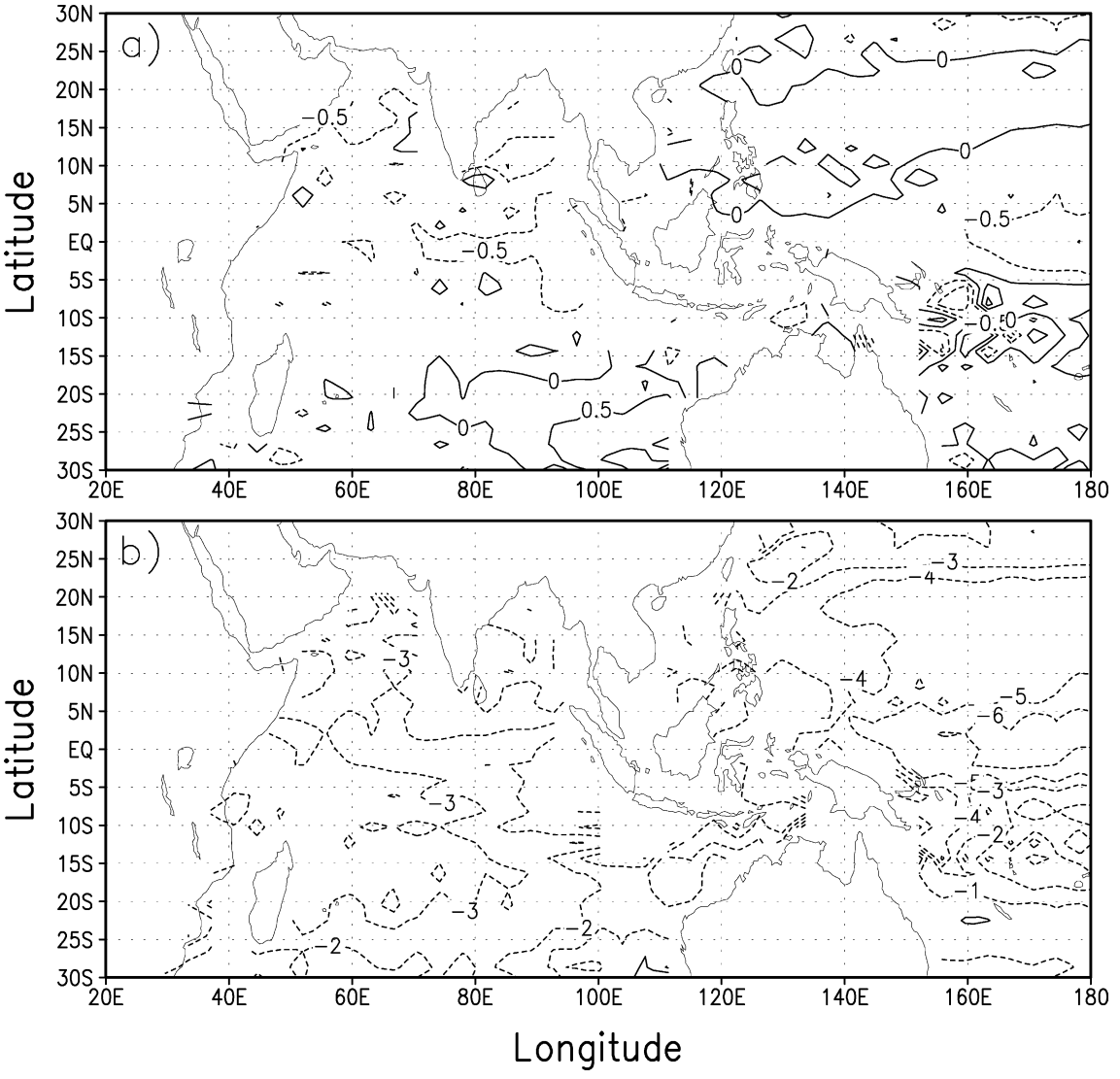

Fig. 10. Annual mean sea surface temperature differences (experiment minus control) (a) in the mid-Holocene and (b) at the LGM. Units are °C and the contour interval is 0.5 °C in (a) and 1 °C in (b).

During the mid-Holocene, increased snowfall in the northwestern Himalaya (Fig. 9b) correlates with increased wind convergence over the region (cf. Fig. 8b), particularly at the start of the winter monsoon season. Simulated annual mean snow accumulation is greater both during the mid-Holocene and at the LGM, and so the model's surface albedo is therefore greater over a larger area in both simulations. A component of the monsoon feedback is therefore likely to be caused by the large-scale response of the atmosphere to this change in surface albedo (Bush, 2000). In fact, increased convergence over the northwestern Himalaya at the start of the winter monsoon in the mid-Holocene simulation is similar to that caused solely by a change in surface albedo over the Himalaya (see Fig. 5c in Bush, 2000).

There is thus spatial variability to the pattern of snow deposition, with largest accumulations in the east at the LGM and largest accumulations in the northwest during the mid-Holocene. Although an explicit snow–firn–ice transition is not incorporated into this model, these simulated differences nevertheless imply a spatial variability in the amount of ice buildup that would have occurred during these two time periods.

There is some agreement of these model results with field studies conducted in the Himalaya. At Nanga Parbat in the northwestern Himalaya, glaciers expanded during the relatively warm and moist early–mid-Holocene climate (Phillips et al., 2000; Richards et al., 2000) whereas at the LGM, expansion in the eastern Himalaya was dominant (Richards et al., 2000). Increased accumulation in the eastern Himalaya at the LGM is also consistent with a stronger westerly component of the summer monsoon winds, as suggested by the distribution of aeolian sediments in the Arabian Sea (Sirocko et al., 1991) as well as by the monsoon winds simulated here (cf. Fig. 2c). There is still excess snow accumulation simulated in the northwestern Himalaya at the LGM, although it is smaller than in the east. From field data, it appears that there was some degree of glacier expansion in this region at the LGM, although it was less than in the Holocene (Phillips et al., 2000; Taylor and Mitchell, 2000).

The impact of Pacific SST on the monsoon circulation may be inferred from the pattern of annual mean wind anomalies (cf. Fig. 8) and differences in annual mean SST (Fig. 10). In the mid-Holocene simulation, the Indian Ocean is cooler than in the control simulation by approximately 0.5°. This cooling induces relatively high pressure and the anticyclonic circulation anomalies that are evident in the annual mean wind differences (Fig. 8b). In the LGM simulation, Indian Ocean SSTs are ~3° colder than today, but the wind response is complicated by the fact that the Sunda shelf is exposed and that convection there dominates the response. Increased surface easterlies over the far western Pacific, however, play a role in converging winds into the southerly jet that flows into the eastern Himalaya. SST in the tropical Pacific can therefore play a regulatory role in both the strength of this jet and in the available moisture that it can precipitate out as snow.

6. Conclusions

It has been shown that in a coupled atmosphere–ocean GCM, the simulated South Asian monsoon was different from today's, both during the mid-Holocene and at the LGM. Seasonal differences show that the speed and direction of the LGM monsoon winds were quite different and that during the summer monsoon the flux of Arabian lithogenic sediments into the northwestern Arabian Sea would have increased. Reduction in annual mean upwelling in the northwest Arabian Sea occurs in the LGM simulation, but farther northeast, near the Gulf of Oman, upwelling is similar to, if not stronger than, today.

Wind changes during the mid-Holocene, on the other hand, were smaller but induced much stronger coastal upwelling. SST changes are shown to be responsible in part for the changes in annual mean circulation patterns, although there are other competing factors (particularly at the LGM).

Simulated snow accumulation agrees with proxy data gathered from the Himalaya, which indicate increased accumulation in the northwestern Himalaya during the mid-Holocene and increased accumulation in the eastern Himalaya at the LGM. The asynchroneity between Himalayan glacier expansion and Northern Hemisphere ice sheet volume may therefore be due in part to the circulation changes described here.

One important outcome of model–data intercomparisons is that they may be used to constrain the spatio-temporal variability of past climate change, and hence they may be helpful in the interpretation

of paleoclimatic data. While higher resolution models or statistical downscaling techniques would be required for more regional intercomparisons, climate models can nevertheless be useful in diagnosing and explaining observed variability in bulk climatic quantities over relatively large regions, and further, they can assist in the assessment of the global impact of such variability.

Acknowledgements

The author thanks the Natural Sciences and Engineering Research Council for support through Research Grant OGP0194151 and the Climate System History and Dynamics Project, as well as UNESCO for sponsoring International Geological Correlation Project 415. The author is most appreciative to Doug Benn and Jack Schroder for their useful comments on a previous version of the manuscript.

References

Benn, D.I., Owen, L.A., 1998. The role of the Indian summer monsoon and the mid-latitude westerlies in Himalayan glaciation: review and speculative discussion. J. Geol. Soc. 155, 353–363.

Berger, A., 1992. Orbital variations and insolation database, IGBP PAGES/World Data Center-A for Paleoclimatology Data Contribution Series #92-007. NOAA/N GDC Paleoclimatology Program, Boulder, CO, USA.

Berger, A., Loutre, M.F., 1991. Insolation values for the climate of the last 10 million years. Quat. Sci. Rev. 10, 297–317.

Bush, A.B.G., 1999. Assessing the impact of mid-Holocene insolation on the atmosphere–ocean system. Geophy. Res. Lett. 26, 99–102.

Bush, A.B.G., 2000. A positive feedback mechanism for Himalayan glaciation. Quat. Int. 65-6, 3–13.

Bush, A.B.G., Philander, S.G.H., 1998. Tropical cooling in a coupled model simulation of the Last Glacial Maximum. Science 279, 1341–1344.

Bush, A.B.G., Philander, S.G.H., 1999. The climate of the Last Glacial Maximum: results from a coupled atmosphere–ocean general circulation model. J. Geophys. Res. 104, 24509–24525.

Clemens, S.C., Prell, W.L., 1990. Late Pleistocene variability of Arabian Sea summer-monsoon winds and dust source-area aridity: a record from the lithogenic component of deep-sea sediments. Paleoceanography 5, 109–145.

Climate: Long-Range Investigation, Mapping, and Prediction (CLIMAP) 1981. Project Members, Seasonal reconstructions of the Earth's surface at the last glacial maximum, Map and Chart Series MC-36, Geol. Soc. Am., Boulder, CO.

Cullen, J.L., 1981. Microfossil evidence for changing salinity patterns in the Bay of Bengal over the last 20,000 years. Palaeogeogr., Palaeoclimatol., Palaeoecol. 35, 315–356.

Dey, B., Bhanu Kumar, O.S.R.U., 1982. An apparent relationship between Eurasian spring snow cover and the advance period of the Indian summer monsoon. J. Appl. Meteorol. 21, 1929–1932.

Dey, B., Kathuria, S.N., Bhanu Kumar, O.S.R.U., 1985. Himalayan summer snow cover and withdrawal of the Indian summer monsoon. J. Clim. Appl. Metereol. 24, 865–868.

Dickson, R.R., 1984. Eurasian snow cover versus Indian monsoon rainfall—an extension of the Hahn-Shukla results. J. Clim. Appl. Metereol. 23, 171–173.

Fairbanks, R.G., 1989. A 17,000-year glacio-eustatic sea level record: influence of glacial melting rates on Younger Dryas event and deep-ocean circulation. Nature 342, 637–642.

Fanning, A.F., Weaver, A.J., 1996. An atmospheric energy–moisture balance model: climatology, interpentadal climate change, and coupling to an ocean general circulation model. J. Geophys. Res. 101, 15111–15128.

Gordon, C.T., Stern, W., 1982. A description of the GFDL global spectral model. Mon. Weather Rev. 110, 625–644.

Guilderson, T.P., Fairbanks, R.G., Rubenstone, J.L., 1994. Tropical temperature variations since 20,000 years ago: modulating interhemispheric climate change. Science 263, 663–665.

Hahn, D.G., Shukla, J., 1976. An apparent relationship between Eurasian snow cover and Indian monsoon rainfall. J. Atmos. Sci. 33, 2461–2462.

Keshavamurty, R.N., 1982. Response of the atmosphere to sea surface temperature anomalies over the equatorial Pacific and the teleconnections of the Southern Oscillation. J. Atmos. Sci. 39, 1241–1259.

Kutzbach, J.E., Guetter, P.J., 1986. The influence of changing orbital parameters and surface boundary conditions on climate simulations for the past 18,000 years. J. Atmos. Sci. 43, 1726–1759.

Kutzbach, J.E., Otto-Bliesner, B.L., 1982. The sensitivity of the African–Asian monsoonal climate to orbital parameter changes for 9000 years B.P. in a low-resolution general circulation model. J. Atmos. Sci. 39, 1177–1188.

Levitus, S., 1982. Climatological atlas of the world ocean. NOAA Prof. Paper 13, US Govt. Print. Office, Washington, DC, 173 pp.

Lyle, M.W., Prahl, F.G., Sparrow, M.A., 1992. Upwelling and productivity changes inferred from a temperature record in the central equatorial Pacific. Nature 355, 812–815.

Meehl, G.A., 1997. The South Asian monsoon and the tropospheric biennial oscillation. J. Clim. 10, 1921–1943.

Metivier, F., Gaudemer, Y., 1999. Stability of output fluxes of large rivers in South and East Asia during the last 2 million years: implications on floodplain processes. Basin Res. 11, 293–303.

Otto-Bleisner, B.L., 1999. El Niño/La Niña and Sahel precipitation during the middle Holocene. Geophys. Res. Lett. 26, 87–90.

Pacanowski, R.C., Dixon, K., Rosati, A., 1991. The GFDL modular ocean model user guide. GFDL Ocean Group Tech. Rep. 2, Geophys. Fluid Dyn. Lab, Princeton, NJ.

Pedersen, T.F., 1983. Increased productivity in the eastern equatorial Pacific during the last glacial maximum (19,000 to 14,000 yr B.P.). Geology 11, 16–19.

Peltier, W.R., 1994. Ice age paleotopography. Science 265, 195–201.

Phillips, W.M., Sloan, V.F., Shroder Jr., J.F., Sharma, P., Clarke, M.L., Rendell, H.M., 2000. Asynchronous glaciation at Nanga Parbat, northwestern Himalaya Mountains, Pakistan. Geology 28, 431–434.

Prell, W.L., 1984. Monsoonal climate of the Arabian Sea during the late Quaternary: a response to changing solar radiation. In: Berger, A., et al., (Eds.), Milankovitch and Climate. Reidel, Dordrecht, pp. 349–366.

Prell, W.L., Kutzbach, J.E., 1992. Sensitivity of the Indian monsoon to forcing parameters and implications for its evolution. Nature 360, 647–652.

Prell, W.L., van Campo, E., 1986. Coherent response of Arabian Sea upwelling and pollen transport to late Quaternary monsoonal winds. Nature 323, 526–528.

Prins, M.A., Postma, G., 2000. Effects of climate, sea level, and tectonics unraveled for last deglaciation turbidite records of the Arabian Sea. Geology 28, 375–378.

Rasmusson, E.M., Carpenter, T.H., 1983. The relationship between eastern equatorial Pacific sea surface temperatures and rainfall over India and Sri Lanka. Mon. Weather Rev. 111, 517–528.

Richards, B.W., Owen, L.A., Rhodes, E.J., 2000. Timing of Late Quaternary glaciations in the Himalaya of northern Pakistan. J. Quat. Sci. 15, 283–297.

Sarnthein, M., Winn, K., 1990. Reconstruction of low and middle latitude export productivity, 30,000 years B.P. to present: implications for global carbon reservoirs. In: Schlesinger, M. (Ed.), Climate Ocean Interaction. NATO ASI Ser. Kluwer Academic Publishing, London, pp. 317–342.

Sarnthein, M., Tetzlaff, G., Koopman, B., Wolter, K., Pflaumann, U., 1981. Glacial and interglacial wind regimes over the eastern subtropical Atlantic and north–west Africa. Nature 293, 193–196.

Shrestha, A.B., Wake, C.P., Dibb, J.E., Mayewski, P.A., 2000. Precipitation fluctuations in the Nepal Himalaya and its vicinity and relationship with some large scale climatological parameters. Int. J. Clim. 20, 317–327.

Sirocko, F., Sarnthein, M., Lange, H., Erlenkeuser, H., 1991. Atmospheric summer circulation and coastal upwelling in the Arabian Sea during the Holocene and the Last Glaciation. Quat. Res. 36, 72–93.

Soman, M.K., Slingo, J., 1997. Sensitivity of the Asian summer monsoon to aspects of sea-surface-temperature anomalies in the tropical Pacific Ocean. Q. J. R. Metereol. Soc. 123, 309–336.

Taylor, P.J., Mitchell, W.A., 2000. The Quaternary glacial history of the Zanskar Range, north–west Indian Himalaya. Quat. Int. 65-6, 81–99.

Torrence, C., Webster, P.J., 1999. Interdecadal changes in the ENSO–monsoon system. J. Clim. 12, 2679–2690.

Wright Jr., H.E., Kutzbach, J.E., Webb, T., Ruddiman, W.F., Street-Perrott, F.A., Bartlein, P.J. (Eds.), 1993. Global Climates Since the Last Glacial Maximum. University of Minnesota Press, Minneapolis, 569 pp.